Biosensors and Bioelectronics 216 (2022) 114642

Contents lists available at ScienceDirect

Biosensors and Bioelectronics

journal homepage: www.elsevier.com/locate/bios

Comparison of electrical and optical transduction modes of DNA-wrapped SWCNT nanosensors for the reversible detection of neurotransmitters.

P. Clément [a,1], J. Ackermann [b], N. Sahin-Solmaz [a], S. Herbertz [b], G. Boero [a], S. Kruss [b,c,*], J. Brugger [a,**]

[a] Microsystems Laboratory, Ecole Polytechnique Fédérale de Lausanne (EPFL), Switzerland
[b] Fraunhofer Institute for Microelectronic Circuits and Systems, Germany
[c] Department of Chemistry, Ruhr-University Bochum, Germany

ARTICLE INFO

Keywords:
Biosensors
Carbon nanotube
Electrical transduction
Molecular recognition
Near-infrared fluorescence
Neurotransmitter

ABSTRACT

In this study, we compare the electrical and optical signal transduction of nanoscale biosensors based on single-walled carbon nanotubes (SWCNTs). Solution processable single-stranded (ss) DNA-wrapped SWCNTs were used for the fabrication of the distinct sensors. For electrical measurements, SWCNTs were assembled from solution onto pre-patterned electrodes by electric-field-assisted assembly in field-effect transistor (FET) configuration. A combination of micro- and nano-fabrication and microfluidics enabled the integration into a sensing platform that allowed real-time and reversible detection. For optical measurements, the near-infrared (NIR) fluorescence of the SWCNTs was acquired directly from solution. The detection of important biomolecules was investigated in high-ionic strength solution (0.5xPBS). Increase in fluorescence intensities correlated with a decrease in the SWCNTs electrical current and enabled detection of the important biomolecules dopamine, epinephrine, and ascorbic acid. For riboflavin, however, a decrease in the fluorescence intensity could not be associated with changes in the SWCNTs electrical current, which indicates a different sensing mechanism. The combination of SWCNT-based electrical and optical transduction holds great potential for selective detection of biomarkers in next generation portable diagnostic assays.

1. Introduction

The development of miniaturized wearable and implantable systems involves increasingly research that is targeted on integrated biosensors based on functional nanomaterials for improved selectivity, sensitivity, power-consumption and cost-efficient manufacturability using sustainable materials and methods. Single-walled carbon nanotubes (SWCNTs) are 1D hollow tubes in which the mass is concentrated on the sidewall of atomically thick graphene-like structures. With a diameter of ~1 nm, their dimensions are close to biological species, ensuring size compatibility between the transducer (here semiconducting SWCNT) and the biological target. Moreover, they are solution processable and thus can be integrated on various substrates (Saha et al., 2014). In recent years, SWCNTs have been intensively explored as nano-bioprobes due to their exceptional electrical and optical properties (Ackermann et al., 2022; Shkodra et al., 2021; Sireesha et al., 2018).

SWCNTs have relatively large carrier mobilities and large surface-to-volume ratios, making them very sensitive to small changes in the electrostatic surface potential induced by the recognition of a target molecule (Heller et al., 2008). To sensitively measure these changes, SWCNT field-effect-transistors (FET) are used, which are based on controlling the flow of charges (electrons or holes) in the SWCNTs channel connecting two conductive electrode terminals (source and drain) with a third electrode (gate). This configuration is particularly suitable for multiplexed *in-vitro* analysis because it allows the assembly of multiple sensors enabling easier on-chip integration and has high sensitivity (Xu et al., 2018). However, it is more invasive for *in-vivo* analysis as the whole device need to be inserted into the body. Besides, semiconducting SWCNTs fluoresce in the near-infrared (NIR, 870–2400 nm), depending on their carbon lattice structure described by the chiral index (*n,m*) (Bachilo et al., 2002; O'Connell et al., 2002). When excited with light, an electron-hole pair (exciton) is created that diffuses along

* Corresponding author. Department of Chemistry, Ruhr-University Bochum, Universitaetsstrasse 150, 44801 Bochum, Germany.
** Corresponding author. Microsystems Laboratory, Ecole Polytechnique Fédérale de Lausanne (EPFL), Station 17, 1015, Lausanne, Switzerland.
E-mail addresses: sebastian.kruss@rub.de (S. Kruss), juergen.brugger@epfl.ch (J. Brugger).
[1] Current affiliation: Centre Suisse d'électronique et de microtechnique (CSEM S.A.), Jaquet-Droz 1, Neuchâtel (Switzerland).

https://doi.org/10.1016/j.bios.2022.114642
Received 8 June 2022; Received in revised form 5 August 2022; Accepted 15 August 2022
Available online 27 August 2022

the SWCNT axis until it recombines radiatively. Since every carbon atom is exposed to the surrounding environment, excitons traveling across the SWCNT surface are affected by local changes in dielectric, polarity, and other perturbation (Ackermann et al., 2022; Nißler et al., 2021; Polo and Kruss, 2016). However, to separate excitation from emission signals, optical devices need to be equipped with appropriate optical filters and a NIR sensitive readout, which can be expensive and challenging as device miniaturization increases. Without an internal reference, they can also be susceptible to ambient light fluctuations. Furthermore, they are adventurous for non-contact readouts. Their NIR radiation falls within the biological transparency window, where increased penetration depths into biological tissues are possible. Therefore, optical SWCNT-based sensors are most suitable for *in-vivo* analysis, but also self-contained processes such as reactor production monitoring. In addition, a high resolution is possible as the fluorescence of a single SWCNT can be measured.

The selective detection of a targeted analyte relies on specific binding to a recognition element that is closely immobilized on the sidewall of the nanotube. In recent years, several surface functionalization strategies were studied, notably by covalent (Clément et al., 2019; Mann et al., 2020; Setaro et al., 2017) and non-covalent approaches. Large biopolymers such as single-stranded (ss)DNA enable stable conjugates due to strong π-π stacking between the nucleobase and the SWCNT allowing dispersion of individual SWCNTs in aqueous solutions (Zheng et al., 2003). Extensive ssDNA-SWCNT analyte screenings have demonstrated that certain ssDNA-SWCNTs can be quite specific without the need to use expensive detection units like antibodies (Zhang et al., 2013). Thus, ssDNA-SWCNT-based sensors have already been identified for a variety of analytes. For example, several ssDNA functionalizations exist for optical SWCNT detection of neurotransmitters (Beyene et al., 2019; Elizarova et al., 2022; Kruss et al. 2014, 2017b), but no comparison has yet been made to determine whether an identified functionalization can be transferred between optical and electrical SWCNT readout.

We exemplarily chose a SWCNT-based sensor already well studied for optical neurotransmitter detection to investigate the electrical and optical response when exposed to dopamine, ascorbic acid, riboflavin, and epinephrine in physiological buffer (PBS) and compared the sensing mechanisms.

2. Material and methods

2.1. DNA-wrapping of the SWCNTs

Surface modification of (6,5) chirality-enriched CoMoCAT-SWCNTs (Sigma-Aldrich, product no. 773735) with $(GT)_{10}$ ssDNA was performed by following a recently published protocol (Nißler et al., 2019). 100 µl of SWCNTs (2 mg/ml in 1× PBS) were mixed with 100 µl of ssDNA (2 mg/ml in 1× PBS), tip-sonicated in an ice bath (10 min at 30% amplitude/36 W output power, Fisherbrand Model 120 Sonic Disembrator), and then centrifuged (2 × 30 min, 16100 g, 4 °C) to remove aggregates and remaining metal catalysts from SWCNT synthesis. The supernatant yielded the sensor material for further experiments. Control experiment of the SWCNTs wrapped with DNA and dispersed with a surfactant is shown in Fig. SI 1.

2.2. Fabrication of the sensing platform for electrical measurements

The sensing platform is composed of a silicon chip, a PDMS microfluidic cell, a 3D printed cover and an anodized aluminium holder. The silicon chip was fabricated at the Center of Micro and Nanotechnology (CMi) at EPFL. A scheme of the sensing platform with all the individual parts is shown in Fig. SI 2 and fabrication details in the supporting information (Fig. SI 3–4).

2.3. Immobilization of DNA-SWCNTs

(6,5)-enriched $(GT)_{10}$-SWCNTs were diluted 800× (concentration circa 0.15 nM) and dialyzed in water with 20 K MWCO MINI Dialysis polypropylene cups (Thermofisher) overnight. They were assembled from solution onto pre-patterned electrodes by electric-field-assisted assembly (also called dielectrophoresis) A drop (5 µL) was casted on the silicon chip and an alternative voltage of 2 V at 400 kHz during 30 s was applied. These conditions were optimized to immobilize few tens of SWCNTs. The sample was washed with DI water and blown with dry air (Fig. SI 6). For the control experiment, bare SWCNTs dispersed in water with 1% of SDS were immobilized onto pre-patterned electrodes following the same procedure.

2.4. Electrical measurements setup

A low noise transimpedance amplifier was designed in-house to measure the current signal of the SWCNTs-FET. The amplifier consists of two stages, a current-to-voltage converter and a non-inverting voltage gain. Detailed schematic of the transimpedance amplifier similar to that reported in (Chavarria et al., 2017), is shown in Fig. SI 4 of the SI.

2.5. Optical measurements setup

The NIR fluorescence setup consisted of a CMOS camera (Orca Flash 4.0 Hamamatsu) connected to an inverted microscope (Nikon Eclipse Ti2) equipped with a 10× objective. A white LED was used in combination with a 560 ± 40 nm bandpass filter for excitation of SWCNTs via the E_{22} transitions. Excitation light was eliminated from emission via an 840 nm long-pass filter.

For NIR fluorescence response measurements of the analytes, $(GT)_{10}$-SWCNTs were diluted in 0.5× PBS to a concentration of 0.7 nM which is the concentration calculated based on previous literature (Nißler et al., 2019; Sanchez et al., 2016; Schöppler et al., 2011; Streit et al., 2014). 2 µl of the corresponding and freshly prepared analyte solutions (1 mM) in 0.5× PBS were added to 200 µl of the diluted SWCNT solution in a 96-well plate, resulting in an analyte concentration of 10 µM. During this time course, images were captured with an integration time of 1 s. Relative fluorescence intensity changes in comparison to no analyte addition were analyzed based on an area of 500 pixels in the center of the sensor solution image and averaged from triplicates.

For characterization SWCNT dispersion, absorption spectra were recorded using a JASCO V-780-ST spectrophotometer in the wavelength range of 400–1350 nm in 2 nm steps in disposable plastic cuvettes (Brand, 10 mm optical path). Zeta potential measurements were carried out using a Zetasizer Nano ZS (Malvern Instruments, UK) in 0.5× PBS at SWCNT concentrations of 0.7 nM with and without addition the corresponding analytes (ascorbic acid, epinephrine, dopamine, riboflavin) at a concentration of 10 µM (Fig. SI 5).

3. Results

The fabrication of the electrical biosensors combines top-down (photolithography) and bottom-up (assembly) strategies as described in the material and method section. Our approach is based on a single-step and environmentally friendly assembly of DNA-SWCNTs onto silicon substrate with patterned electrodes fabricated by photolithography (see SI). (6,5)-enriched semiconducting SWCNTs were functionalized by physisorption with $(GT)_{10}$ ssDNA (Fig. 1a) for two purposes. First, it allows the dispersion of individual SWCNTs in solution via π-π stacking interaction with the side wall (Fig. 1b) and secondly, it is known to interact with some neurotransmitters where the hydroxy groups interact with the phosphate groups of the DNA (Kruss et al., 2017a; Polo and Kruss, 2016). AFM imaging shows that a typical small bundle of $(GT)_{10}$-SWCNTs was immobilized by dielectrophoresis between two electrodes (source and drain) with a gap of around 600 nm in FET

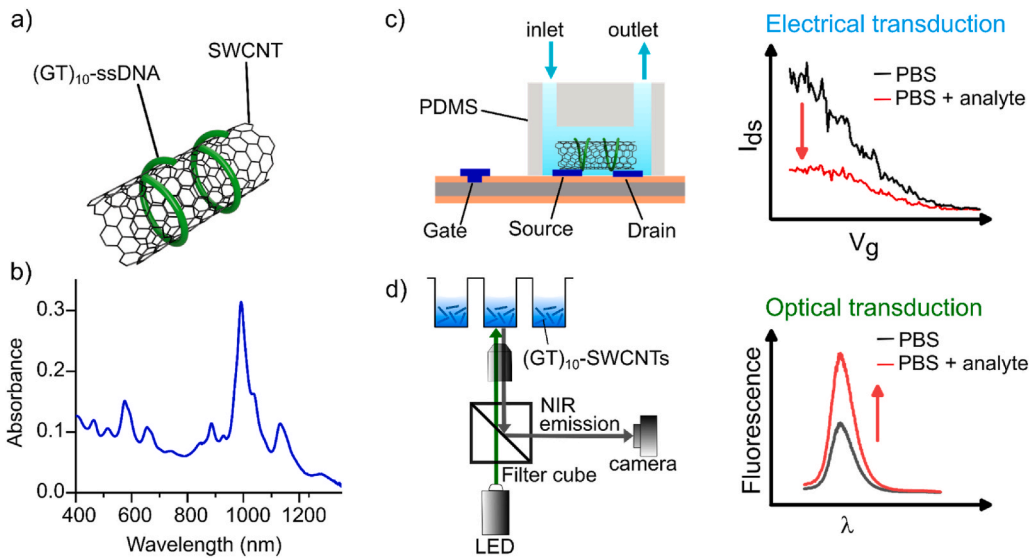

Fig. 1. Electrical and optical transduction principle of DNA-wrapped SWCNT sensors. a) SWCNTs are wrapped with single-stranded $(GT)_{10}$ DNA to render them sensitive as a sensor for biomolecules such as neurotransmitters. b) Absorbance of $(GT)_{10}$-SWCNTs individually dispersed in PBS, c) Electrical sensing platform with an integrated microfluidic system. SWCNTs are immobilized via dielectrophoresis between two electrodes (source and drain). Upon a sensing event a change in current results between drain and source (I_{ds}). d) Optical setup equipped with necessary filters to detect the NIR fluorescence of $(GT)_{10}$-SWCNTs in solution. A sensing event results in a change in fluorescence intensity.

configuration (see Fig. SI 6). The cross-section profile indicates that the thickness ranges from 1.5 to 6 nm which corresponds to 1 to 4 SWCNT diameters. The device was incorporated into an in-house designed sensing platform coupled with a microfluidic system and a transimpedance amplifier PCB with a Labview interface for current measurements down to the nA range (Fig. 1c, see also SI). The real-time and reversible detection of dopamine, epinephrine, ascorbic acid and riboflavin was investigated in 0.5× PBS solution. The same batch of $(GT)_{10}$-SWCNTs was also placed in a 96-well plate and excited at a wavelength of 560 nm. The fluorescence intensity variation was recorded by a CMOS camera (Fig. 1d).

$(GT)_{10}$-SWCNTs electrical response variations were recorded upon addition of 10 μM of the different analytes (Fig. 2 a,c); Drain-source voltage (V_{ds}) and gate-to-source voltage (V_g) were kept constant at 50 mV and −500 mV, respectively. The drain-source current (I_{ds}) decreased significantly in the presence of dopamine, ascorbic acid and epinephrine to reach a plateau after circa 100 s, and recovered when 0.5× PBS was subsequently added (see also Fig. SI 7). No significant variation was observed with riboflavin, a neuroprotective agent. A control experiment with bare SWCNTs in real-time detection showed no electrical signal variation when injecting 1 mM of each analyte (Fig. SI 8).

In addition, optical measurements were performed with the same sensors. For this purpose, the sensor change was measured analogously to the electrical measurements in 0.5× PBS with the addition of 10 μM

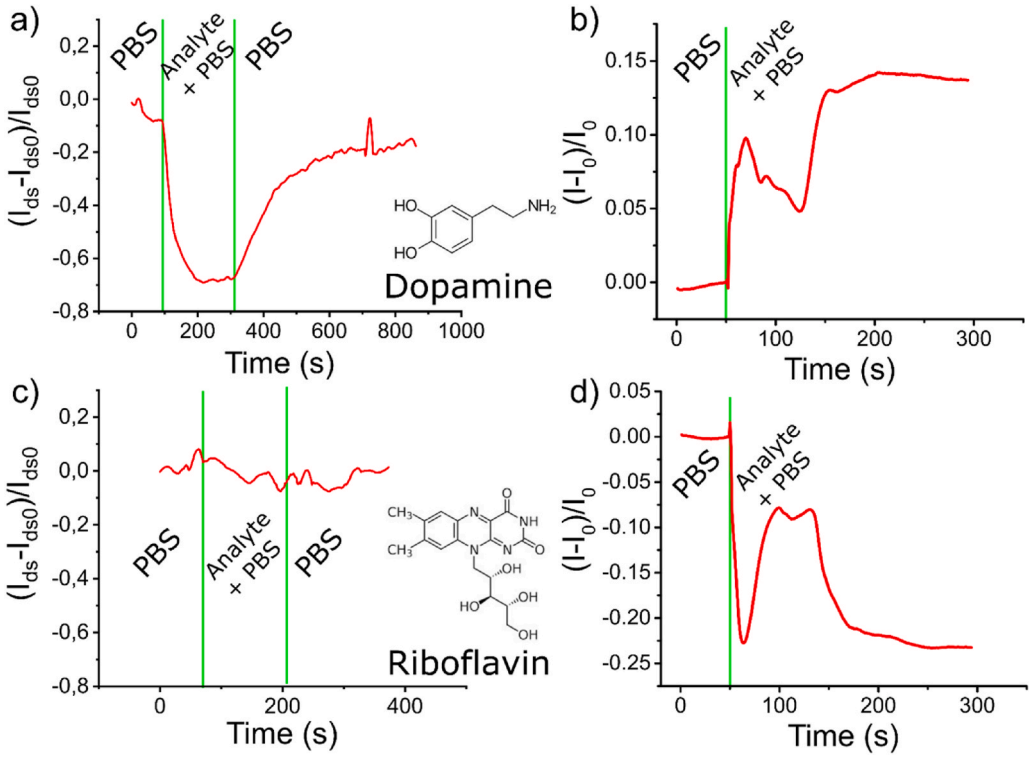

Fig. 2. Real-time detection of analytes in electrical and optical configuration. 10 μM of a-b) dopamine and c-d) riboflavin. "PBS" region corresponds to the injection of 0.5xPBS and "Analyte + PBS" region to the injection of 0.5xPBS + analyte (separated by a green line). V_{ds} = 50 mV and V_g = −500 mV.

analyte. In contrast to electrical measurements, analytes were manually pipetted into the sensor solution. This initially resulted in intensity fluctuations due to the presence of the pipette and the non-uniformity of analyte distribution in the well, but stabilized, when diffusion of the analyte throughout the entire microwell is complete. After addition of dopamine, epinephrine or ascorbic acid (Fig. 2b, SI7), an increase in fluorescence intensity was observed that reached a stable plateau after 250 s. In the case of riboflavin injection, the optical response showed a decrease in fluorescence intensity (Fig. 2d). The reversible detection is not shown in this work and was demonstrated in previous studies (Kruss et al. 2014, 2017b). A control experiment of the SWCNTs optical signal stability in 0.5× PBS buffer was recorded and showed less than 2% of drift for a typical detection time frame (Figure SI9).

A comparison of the normalized optical and electrical responses is established in Fig. 3a. Notably, an increase in fluorescence intensity was correlated to a decrease in the SWCNTs electrical current for the detection of dopamine, epinephrine and ascorbic acid. Interestingly, this phenomenon has a linear dependence as shown in Fig. 3b. A different behavior is observed for riboflavin where a decrease in the fluorescence intensity is not associated with a change in the electrical current.

4. Discussion

In the literature, both optical and electrical SWCNT sensors can be found for a broad range of analytes. However, the electrical and optical transduction mechanisms have never been compared in identical conditions (i.e., same analytes and concentrations). This comparison could however contribute to a better understanding of the detailed transduction mechanism in SWCNT-based sensors and, in case that both sensing pathways are identical could allow the user for choosing which variation (electrical or optical) is better suited for the application.

From a physical point of view, SWCNT-based FETs are based on the measurement of the current flow between the source and drain electrodes. Their transport characteristic is known to be affected by the surrounding environment, e.g., by a change in the band bending of the CNTs themselves or by the metal contacts, resulting in a change of the current (Heller et al., 2008). In contrast, the signal change of optical SWCNT-based sensors is based on a change in fluorescence due to the decay of excitons, which are also strongly affected by their surrounding environment (Cognet et al., 2007). Therefore, both transduction mechanisms render the SWCNT as a sensitive material for biosensing applications. In the case of dopamine, epinephrine, and ascorbic acid, the correlation of electrical and optical responses suggests that the sensing mechanism is the same, whereas riboflavin may play a special role in optical measurements due to its absorption and emission in the visible range and will be discussed separately below.

Sensing mechanisms with electrostatic gating for FET-SWCNTs based biosensors have been discussed by Heller et al., (2008) where they summarized three common mechanisms upon adsorption of proteins: electrostatic gating, Schottky barrier and gate capacitance reduction due to the low permittivity of the solution. In our experiment we used 0.5× PBS buffer therefore we do not have a variation in the ionic strength of the solution avoiding gate capacitance reduction. The sensing mechanism of our biosensor is most likely influenced by the electrostatic gating and Schottky barrier mechanism. The latter arises from changes in the metal work function due to adsorbed molecules and consequently a change in band alignment. However, the optical measurements are performed with SWCNTs without metal contacts and, consequently, cannot be affected by Schottky barrier changes in their optical properties. Electrostatic gating implies an opposite charge change/doping of the SWCNTs induced by the attachment of charged molecules and correlates also with assumptions of a change in charge distribution in optical measurements (Kruss et al., 2017a). Therein, it has been shown that a complex interplay between electrostatic interactions of the molecule with the organic phase around the SWCNT is likely to determine the observed sensitivity and selectivity of the respective sensors(Harvey et al., 2018; Mann et al., 2017).

At the physiological conditions under which our measurements were made, dopamine and epinephrine are predominantly cationic, thus positively charged due to protonated amino groups, while ascorbic acid is anionic due to deprotonated hydroxyl groups at the ring system (Berfield et al., 1999; Shao and Venton, 2022). Therefore, possible mechanisms for electrostatic gating exist: SWCNTs showed a p-type behavior and are wrapped with DNA that possesses a negatively charged phosphate backbone. When a negative voltage is applied between the gate electrode and the source electrode, positive charges are generated at the interface of the gate electrode while negative charges (anions from the solution) accumulate at the interface between the SWCNT and the electrolyte. In solution, this region is characterized as the electrical double layer (EDL) where an exponential decay of ions from the nanotube to the solution is observed at a distance λ_D referred to as the Debye length (around 1 nm in our study). Therefore, a decrease in I_{ds} current is associated with a decrease of positive charges through the nanotube and is induced by a decrease of the negative charge density close to the nanotube. To further support this assumption, zeta potential measurements of $(GT)_{10}$-SWCNTs before and after addition of the respective analytes were performed (Fig. SI 3), showing that a change in the overall charge distribution affect signal changes.

Since 80% of the nanotube surface is covered with DNA (Polo and Kruss, 2016), one can assume that this electrical change is mainly due to the delocalization of the DNA further away from the SWCNT side wall due to DNA conformation changing during the sensing event. Additionally, positively charged dopamine and epinephrine might screen the negatively charged DNA phosphate backbone compared to ascorbic acid which is negatively charged. It results in a stronger electrical signal change for dopamine and epinephrine compared to ascorbic acid.

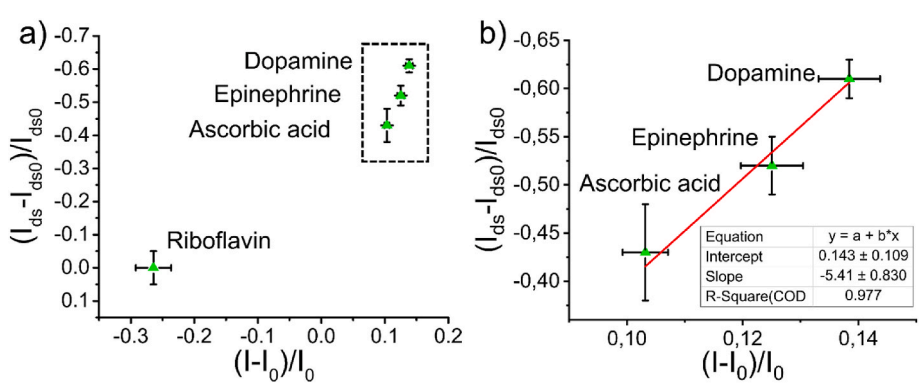

Fig. 3. Comparison of electrical and optical sensor response. a) Electrical (ordinates) versus optical response (abscissae) for the detection of 10 μM of the different analytes. Note that riboflavin does show a NIR fluorescence but not an electrical response. b) Correlation and linear regression of dopamine, epinephrine and ascorbic acid sensor response from the zoom-in window in a). Errors are standard deviations (n = 3).

However, this is contradictory to molecular dynamic simulations that have shown that the DNA is pulled closer to the SWCNT surface by the interaction of the hydroxy groups of dopamine with the DNA backbone (Kruss et al., 2017a). One explanation could be that even though the analyte causes a local pulling of DNA, the rest of the DNA strand also undergoes a conformational change, leading to an overall different displacement of DNA and charges. The general correlation between optical and electrical measurements of dopamine, epinephrine and ascorbic acid thus strengthens the assumption that a change in the charge distribution of the SWCNT due to a conformational change of the corona plays an important role in sensor response.

In contrast, the presence of riboflavin did not induce a change in the electrical response of the carbon nanotube suggesting a different sensing mechanism. Due to π-π stacking, riboflavin is likely to have a particular affinity for the SWCNT surface itself, e.g. it has been used as a fluorophore for measuring the accessible SWCNT area at different coronas (Park et al., 2019). Due to the molecular structure, this direct absorption at the surface is probably different from the interactions of the other analytes studied, suggesting rather a direct quenching of the SWCNTs fluorescence, at a steady state in the charge distribution at its surface. However, as mentioned above, riboflavin could also behave differently in optical measurements due to its light absorption (maximum at 520 nm) and fluorescence (500–580 nm) in the visible region, where SWCNTs also absorb light.

It is known that riboflavin acts as a photosensitizer for singlet oxygen and super oxygen generation, when excited with ultraviolet or visible light, resulting in subsequent degradation of riboflavin(Sen et al., 2012). This is consistent with an observed quenching of the SWCNTs fluorescence from such reactive oxygen species (ROS) and a restored SWCNT fluorescence when trolox, a free radical scavenger, was added, as well as observed quenching of riboflavin with concomitant quenching of SWCNT fluorescence when both were excited in solution (Park et al., 2019). Contradictory to this are the observations from Polo and Kruss, who observed an emission enhancement of riboflavin in the presence of ssDNA-SWCNTs, which could be explained by an energy transfer (Polo and Kruss, 2016) from SWCNT to riboflavin. Here, the addition of known ROS scavengers showed only little effect on fluorescence changes. However, differences in the singlet oxygen formation could also depend on the O_2 conditions during the experiments, which should be specifically controlled for comparable results.

5. Conclusion

We studied the sensing mechanism of DNA-wrapped SWCNTs nanosensors by comparing their optical and electrical transduction modes. A solution processable method with individually dispersed SWCNTs was used for the fabrication of the sensors. SWCNTs were assembled from solution to surface in nanoscale device configuration coupled to a sensing platform with a microfluidic system for real-time electrical signal measurements and reversible detection. We have demonstrated that an increase in fluorescence intensity was correlated to a decrease in the SWCNTs electrical current for the detection of dopamine, epinephrine and ascorbic acid. These findings highlight that there are common signal transduction mechanisms. While optical sensors have the potential for non-contact readout e.g. as *in-vivo* sensors, electrical sensors allow easier on-chip integration. Correlation of signal responses opens up freedom of choice in sensor design between these two readout technologies for the development of the next generation of portable, point of care and home diagnostic assays for the continuous monitoring of different health parameters.

CRediT authorship contribution statement

P. Clément: Conceptualization, Software, Formal analysis, Methodology, Validation, Visualization, Writing – original draft, Project administration. **J. Ackermann:** Methodology, Validation, Formal analysis, Investigation, Resources, Writing – review & editing. **N. Sahin-Solmaz:** Methodology, Resources, Writing – review & editing. **S. Herbertz:** Methodology, Writing – review & editing. **G. Boero:** Software, Validation, Supervision, Writing – review & editing. **S. Kruss:** Funding acquisition, Supervision, Writing – review & editing. **J. Brugger:** Funding acquisition, Supervision, Writing – review & editing.

Declaration of competing interest

The authors declare that they have no known competing financial interests or personal relationships that could have appeared to influence the work reported in this paper.

Data availability

Data will be made available on request.

Acknowledgement

We thank Jonathan Cottet for his valuable technical support with the microfluidic setup and sensing platform fabrication. This work was partially funded by the Deutsche Forschungsgemeinschaft (DFG, German Reuter Foundation) under Germany's Excellence Strategy – EXC 2033–390677874 – RESOLV. This work is supported by the Center for Solvation Science ZEMOS" funded by the German Federal Ministry of Education and Research BMBF and by the Ministry of Culture and Research of Nord Rhine- Westphalia Funded by the VW foundation. This work was supported by the Fraunhofer Internal Programs under Grant No. Attract 038-610097. Part of the funding came from the European Research Council (ERC) under the European Union's Horizon 2020 research and innovation program (ERC-2016-ADG, Project "MEMS 4.0" Grant 742685.

Appendix A. Supplementary data

Supplementary data to this article can be found online at https://doi.org/10.1016/j.bios.2022.114642.

References

Ackermann, J., Metternich, J.T., Herbertz, S., Kruss, S., 2022. Angew. Chem. Int. 61 (18), e202112372.
Bachilo, S.M., Strano, M.S., Kittrell, C., Hauge, R.H., Smalley, R.E., Weisman, R.B., 2002. Science 298 (5602), 2361–2366.
Berfield, J.L., Wang, L.C., Reith, M.E.A., 1999. J. Biol. Chem. 274 (8), 4876–4882.
Beyene, A.G., Delevich, K., Del Bonis-O'Donnell, J.T., Piekarski, D.J., Lin, W.C., Thomas, A.W., Yang, S.J., Kosillo, P., Yang, D., Prounis, G.S., Wilbrecht, L., Landry, M.P., 2019. Science Advances 5 (7), eaaw3108.
Chavarria, M.A., Matheoud, A.V., Marmillod, P., Liu, Y., Kong, D., Brugger, J., Boero, G., 2017. Rev. Sci. Instrum. 88 (3), 035115.
Clément, P., Trinchera, P., Cervantes-Salguero, K., Ye, Q., Jones, C.R., Palma, M., 2019. ChemPlusChem 84 (9), 1235–1238.
Cognet, L., Tsyboulski, D.A., Rocha, J.-D.R., Doyle, C.D., Tour, J.M., Weisman, R.B., 2007. Science 316 (5830), 1465–1468.
Elizarova, S., Chouaib, A.A., Shaib, A., Hill, B., Mann, F., Brose, N., Kruss, S., Daniel, J.A., 2022. Proceedings of the National Academy of Sciences 119 (22), e2202842119.
Harvey, J.D., Zerze, G.H., Tully, K.M., Mittal, J., Heller, D.A., 2018. The Journal of Physical Chemistry C 122 (19), 10592–10599.
Heller, I., Janssens, A.M., Männik, J., Minot, E.D., Lemay, S.G., Dekker, C., 2008. Nano Lett 8 (2), 591–595.
Kruss, S., Landry, M.P., Vander Ende, E., Lima, B.M.A., Reuel, N.F., Zhang, J., Nelson, J., Mu, B., Hilmer, A., Strano, M., 2014. J. Am. Chem. Soc. 136 (2), 713–724.
Kruss, S., Salem, D.P., Vuković, L., Lima, B., Ende, E.V., Boyden, E.S., Strano, M.S., 2017a. Proceedings of the National Academy of Sciences 114 (8), 1789–1794.
Kruss, S., Salem, D.P., Vuković, L., Lima, B., Vander Ende, E., Boyden, E.S., Strano, M.S., 2017b. Proceedings of the National Academy of Sciences 114 (8), 1789–1794.
Mann, F.A., Herrmann, N., Meyer, D., Kruss, S., 2017. Sensors 17 (7), 1521.
Mann, F.A., Herrmann, N., Opazo, F., Kruss, S., 2020. Angew. Chem. Int. Ed. 59 (40), 17732–17738.
Nißler, R., Kurth, L., Li, H., Spreinat, A., Kuhlemann, I., Flavel, B.S., Kruss, S., 2021. Anal. Chem. 93 (16), 6446–6455.
Nißler, R., Mann, F.A., Chaturvedi, P., Horlebein, J., Meyer, D., Vuković, L., Kruss, S., 2019. The Journal of Physical Chemistry C 123 (8), 4837–4847.

O'Connell, M.J., Bachilo, S.M., Huffman, C.B., Moore, V.C., Strano, M.S., Haroz, E.H., Rialon, K.L., Boul, P.J., Noon, W.H., Kittrell, C., Ma, J., Hauge, R.H., Weisman, R.B., Smalley, R.E., 2002. Science 297 (5581), 593–596.
Park, M., Salem, D.P., Parviz, D., Gong, X., Silmore, K.S., Lew, T.T.S., Khong, D.T., Ang, M.C.-Y., Kwak, S.-Y., Chan-Park, M.B., Strano, M.S., 2019. Nano Lett 19 (11), 7712–7724.
Polo, E., Kruss, S., 2016. The Journal of Physical Chemistry C 120 (5), 3061–3070.
Saha, A., Jiang, C., Martí, A.A., 2014. Carbon 79, 1–18.
Sanchez, S.R., Bachilo, S.M., Kadria-Vili, Y., Lin, C.-W., Weisman, R.B., 2016. Nano Lett 16 (11), 6903–6909.
Schöppler, F., Mann, C., Hain, T.C., Neubauer, F.M., Privitera, G., Bonaccorso, F., Chu, D., Ferrari, A.C., Hertel, T., 2011. The Journal of Physical Chemistry C 115 (30), 14682–14686.
Sen, F., Boghossian, A.A., Sen, S., Ulissi, Z.W., Zhang, J., Strano, M.S., 2012. ACS Nano 6 (12), 10632–10645.
Setaro, A., Adeli, M., Glaeske, M., Przyrembel, D., Bisswanger, T., Gordeev, G., Maschietto, F., Faghani, A., Paulus, B., Weinelt, M., Arenal, R., Haag, R., Reich, S., 2017. Nature Communications 8, 14281.
Shao, Z., Venton, B.J., 2022. J. Electrochem. Soc.
Shkodra, B., Petrelli, M., Angeli, M.A.C., Garoli, D., Nakatsuka, N., Lugli, P., Petti, L., 2021. Applied Physics Reviews 8 (4), 041325.
Sireesha, M., Jagadeesh Babu, V., Kranthi Kiran, A.S., Ramakrishna, S., 2018. Nanocomposites 4 (2), 36–57.
Streit, J.K., Bachilo, S.M., Ghosh, S., Lin, C.-W., Weisman, R.B., 2014. Nano Lett 14 (3), 1530–1536.
Xu, X., Clément, P., Eklöf-Österberg, J., Kelley-Loughnane, N., Moth-Poulsen, K., Chávez, J.L., Palma, M., 2018. Nano Lett 18 (7), 4130–4135.
Zhang, J., Landry, M.P., Barone, P.W., Kim, J.-H., Lin, S., Ulissi, Z.W., Lin, D., Mu, B., Boghossian, A.A., Hilmer, A.J., Rwei, A., Hinckley, A.C., Kruss, S., Shandell, M.A., Nair, N., Blake, S., Şen, F., Şen, S., Croy, R.G., Li, D., Yum, K., Ahn, J.-H., Jin, H., Heller, D.A., Essigmann, J.M., Blankschtein, D., Strano, M.S., 2013. Nat. Nanotechnol. 8 (12), 959–968.
Zheng, M., Jagota, A., Semke, E.D., Diner, B.A., McLean, R.S., Lustig, S.R., Richardson, R. E., Tassi, N.G., 2003. Nat. Mater. 2 (5), 338–342.